Core–Shell Structure and Segregation Effects in Composite Droplet Polymer Blends

Joël Reignier and Basil D. Favis
CRASP, Dept. of Chemical Engineering, Ecole Polytechnique, Montreal, QC H3C 3A7 Canada

Core–shell morphology formation within the dispersed phase was studied for composite droplet polymer-blend systems comprising a high-density polyethylene matrix, polystyrene shell and different molecular weights of poly(methyl methacrylate) core material. The blends were prepared in the melt using an internal mixer, and the morphology was analyzed by electron microscopy. Changing the viscoelastic properties of the core in the dispersed phase dramatically affects PS-PMMA segregation within the dispersed composite droplet itself. A high-molecular-weight-PMMA core contains a large quantity of occluded PS inclusions, while the low-molecular-weight PMMA results in a perfectly segregated PS shell and PMMA core. These phenomena were attributed to the viscosity of the PMMA. Using the latter system, a direct microscopic study of the shell formation process demonstrates unambiguously that under conditions of perfect segregation, the onset of complete shell formation corresponds to a shell thickness that is close to two times the radius of gyration of polystyrene. Thus, the thinnest possible shell in such a system possesses a molecular-scale thickness. The system with the high-molecular-weight-PMMA core demonstrates an onset of complete shell formation that is displaced to higher concentrations due to the poor segregation effect. By counterbalancing the effects of viscosity ratio and interfacial effects on the composite droplet size, it is possible to generate perfectly segregated core–shell dispersed-phase morphologies of almost identical size with a controlled shell thickness ranging from 40 to 300 nm.

Introduction

The vast majority of the polymer-blend literature is related to the study of a pure dispersed phase in a matrix system. Another type of structure known as a composite droplet is used to specifically describe the case of a dispersed phase that contains another immiscible polymeric phase. Although very few articles have been dedicated to the examination of such materials, their existence has been known for some time in emulsion systems (Torza and Mason, 1970). Their study, using as-polymerized components, is of great potential, since they indicate a possible route toward next-generation polymer blends where the dispersed phase itself can be controlled as a discrete polymer blend. This approach clearly should allow for a more sophisticated control over the final physical properties of the blend material.

The internal structure within a composite droplet for ternary systems can exhibit different types of morphologies (Figure 1). Hobbs et al. (1988) reported one minor component encapsulating another with a core–shell morphology. Luzinov et al. (1999) introduced the term "multicore structure" to describe the case where several subinclusions of one minor phase are embedded in a larger particle of the second minor phase. In some cases, several authors (Reignier and Favis, 2000; Luzinov et al., 1999) reported the presence of shell subinclusions in the core of the composite droplet.

In binary systems, the presence of subinclusions within the minor phase domains is frequently seen, but rarely discussed. The formation of composite droplet structures in binary poly-

Correspondence concerning this article should be addressed to B. D. Favis.

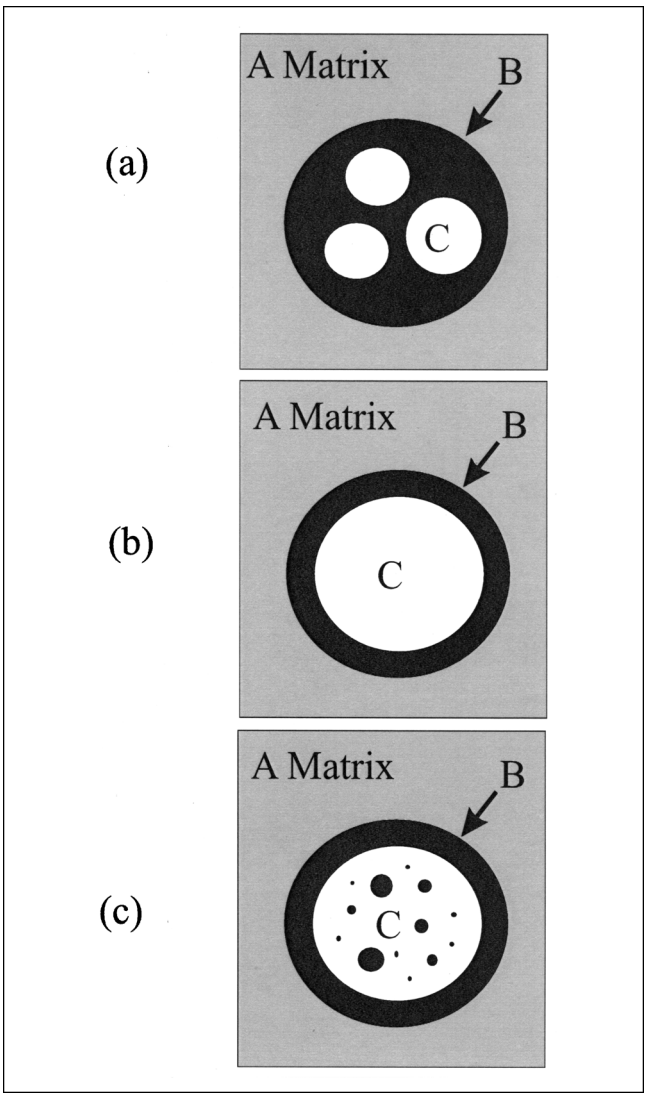

Figure 1. Potential morphologies of a B/C composite droplet in an *A* matrix.

(a) Subinclusions of *C* in a larger domain of *B*; (b) layered particle with *B* shell around *C* core; (c) core–shell structure with shell subinclusions within the core.

mer blends is valuable, as it provides a basis for understanding morphology control of the composite droplet structure in ternary systems, and a review of composite droplet formation in binary blends is given below. In some cases, subinclusion formation is related to viscous effects (Favis and Chalifoux, 1988; Favis et al., 1992), elastic effects (Van Oene, 1972), or both (Berger et al., 1984). Favis et al. (1992) showed that a composite droplet structure could be generated for a 50/50 (vol. %) incompatible binary blend of polypropylene (PP) and polycarbonate (PC) after melt blending near the phase-inversion region, as well as at lower PC concentration (volume fraction = 0.25) by selectively imposing phase inversion and controlling the time of mixing. That system consisted of a PP matrix and PP subinclusions within the more viscous PC dispersed phase. Increasing the viscosity of the dispersed phase (PC) was found to improve the retention of subinclusions with mixing time. In that same work, it was shown that stable subinclusion formation in a binary system could be achieved by combining phase inversion with strong interfacial interactions between the two phases making up the dispersed phase.

In a classic article, Van Oene (1972) showed that, under conditions of dynamic flow, the elasticity differences between the phases in a binary blend can contribute to the interfacial tension. His work emphasizes that a different interfacial tension exists under conditions of dynamic flow and that this dynamic interfacial tension can be quite different from the static one. When the matrix is more elastic than the dispersed phase, the dynamic interfacial tension is lower than the static case. The complementary binary blend results in a system with higher dynamic interfacial tension. Van Oene treated the spontaneous development of subinclusions of the matrix phase in minor phase domains by using this same thermodynamic reasoning and made a calculation of the free energy during flow, taking into account both the number of composite droplets (those containing subinclusions), the number of inclusions inside the composite droplets, and elastic effects. At equilibrium during steady-state flow, the morphology should be depicted by the minimum positive free energy. When the elasticity of the droplet exceeds that of the matrix, the free energy is always positive and is at a minimum when the number of inclusions inside the composite droplets equals zero. Hence, no subinclusions appear under these conditions. However, when the elasticity of the matrix is larger than that of the droplet, subinclusion formation is possible for a dispersed-phase radius greater than a critical value. Surprisingly, in that last case, the formation of subinclusions arises only to obtain a positive value of free energy during flow. This author presented experimental evidence that formation of subinclusions results from elasticity of the components and concluded that for any polymer pair, composite droplets can only be formed by the less elastic phase, but not the other (no matter which component is the minor phase), since this results in a diminution of the overall surface free energy.

Berger et al. (1984) investigated mixtures of different poly(ethylene terephtalate)s with polyamide-6. In particular, they treated the presence of subinclusions of the PET matrix in the PA-6 dispersed phase. When the elasticity of the matrix exceeds that of the droplets, inclusions of the matrix phase are possible in the droplet phase only for large droplets. Furthermore, when the elasticity of the matrix is only slightly greater than that of the dispersed droplet, the elastic effects are negligible and subinclusion formation in that case is considered to be a result of the high-viscosity ratio ($p = 3.7$).

In ternary blends, several authors interpret the presence of shell subinclusions in the core of the composite droplet as a phenomenon reminiscent of the tendency of the core phase to envelop the other minor phase at compositions of the core component higher than the theoretical composition of phase inversion. Luzinov et al. (1999) investigated the morphology of ternary polystyrene/styrene–butadiene rubber/polyethylene (PS/SBR/PE) blends at a constant content of the major component (PS: 75 wt. %) while changing the weight ratio of the minor constitutive polymers. They noticed the presence of SBR subinclusions in the PE dispersed phase (PS is the matrix) at PE contents close to and higher than the theoretical composition of phase inversion for SBR/PE binary blends. It should be pointed out that although the system just eluci-

dated is a composite droplet-type morphology, it falls into a special category since it is just an extension of a typical compatibilized ternary system. Such a system also results in a significant level of interpenetration of each block into the respective pure phases. In another approach, the same trends were also observed by Reignier and Favis (2000) for a HDPE/PS/PMMA ternary blend (three immiscible polymers with no interpenetrating structure). Since some mechanical properties, such as impact strength, of these polymer-blend materials depend critically on the internal structure of core–shell particles (number of subinclusions within the core, shell thickness) (Gupta and Srinivasan, 1993), understanding and controlling the morphology of these complex microstructures is of considerable interest.

It is clear from the preceding work that the state of the art related to understanding and controlling the internal morphology of composite droplet structures is still in its pioneering stage.

This is the third article in a series on composite droplet morphologies in polymer blends (Reignier and Favis, 2000, 2003a). Reignier and Favis (2000) developed characterization techniques and examined a wide range of phenomena related to composite droplet formation for a ternary blend composed of PS and PMMA dispersed in HDPE. In particular, it is shown that all the PMMA in the blend system is present as subinclusions in the PS dispersed phase and that this complex morphology forms within the first minute of mixing and remains stable thereafter. The second article focused on the influence of the molecular weight of the dispersed-phase components on encapsulation effects in the composite droplet phase for PE/PS/PMMA ternary blends. Current models used for predicting encapsulation effects and composite droplet formation in ternary systems (based on static interfacial tension) predict in all cases that PS will encapsulate the PMMA. An unexpected encapsulation of PS by PMMA was observed in one case and was explained by developing a new conceptual model based on dynamic interfacial tension. Calculations based on the dynamic interfacial tension model, using elasticities, based on constant shear stress, were able to account for all of the observed encapsulation effects in that work.

The purpose of this study is to carry out a detailed work related to understanding and controlling the internal structure of composite droplets during melt mixing. Through a detailed study of the influence of the core phase viscosity and its influence on the process of shell formation, a number of questions will be addressed. What are the principal parameters related to core–shell formation? Are core–shell segregation effects an issue, and can they be controlled? What is the smallest possible shell that can be formed? To what extent can the shell thickness, and hence the core–shell morphology, be controlled? What are the breadth of potential structures possible?

Experimental Procedures

Materials

The high-density polyethylene was 4352 N and the polystyrene was 615 APR, both obtained from Dow. The high-molecular-weight poly(methyl methacrylate) (H-PMMA) was IRD-2 obtained from Rohm & Haas, and the low-molecular-weight poly(methyl methacrylate) (L-PMMA) was 20033-6 obtained from Aldrich. A small amount (0.2 wt. %) Irganox B225 antioxidant was added to the mixture to reduce the thermal oxidation of polyethylene. Some of the characteristics of the resins are summarized in Table 1.

Mixing

Melt mixing was carried out in a Haake Rheomix 600 batch mixer with a Haake System 90 drive operating at 200°C and 50 rpm. Using an empirical technique developed by Marquez et al. (1996), the average shear rate in the mixer was estimated to be about 25 s^{-1} with the HDPE matrix. Pellets of the components and antioxidant were premixed by hand before introduction into the mixer. The mass of material added to the mixer was chosen so that a constant volume of roughly 50 cm^3 was achieved for each sample, based on the density measurement at 200°C. After mixing for the required time, the mixer drive was stopped and the front plate was removed, and samples were cut from the mass and dropped directly into a bath of cold water, in order to freeze in the morphology.

Rheological analysis

Rheological characterization of the different polymers was carried out using a Rheometric Scientific constant stress rheometer (SR 5000). The experiments were performed in parallel-plate geometry with a gap of about 1.4 mm under a nitrogen atmosphere at a temperature of 200°C. An oscillation mode at 0.1-Hz frequency was used to control the stability of the raw materials. A stress sweep was also performed to define the region of linear viscoelasticity. The dynamic

Table 1. Material Characteristics

	M_w* $\times 10^{-3}$	M_n* $\times 10^{-3}$	Melt Index** (ASTM)	Density** (g/cm^3) at		$\eta^* \times 10^{-3}$ (Pa·s) at 200°C		$N_1 \times 10^{-4}$ (Pa) at 200°C	
	(g/mol)	(g/mol)	(g/10 min)	20°C	200°C	$\dot{\gamma}$ = cte†	τ = cte††	$\dot{\gamma}$ = cte†	τ = cte††
HDPE	79	24	4	0.962	0.754	1.2	1.2	2.2	2.2
PS	289.8	140.9	15	1.04	0.969	1.7	2.6	11	5.1
H-PMMA	76.5	46.8	5.5	1.19	1.0‡	7.1	26	53	2.2
L-PMMA	11.9	7.8	—	—	1.0	0.043	0.045	0.021	0.6

*Measured by GPC.
**Obtained from suppliers.
†Average shear rate during blending: $\dot{\gamma} = 25\ s^{-1}$.
††Average shear stress during blending: $\tau = 2.7 \times 10^4$ Pa.
‡At 230°C.

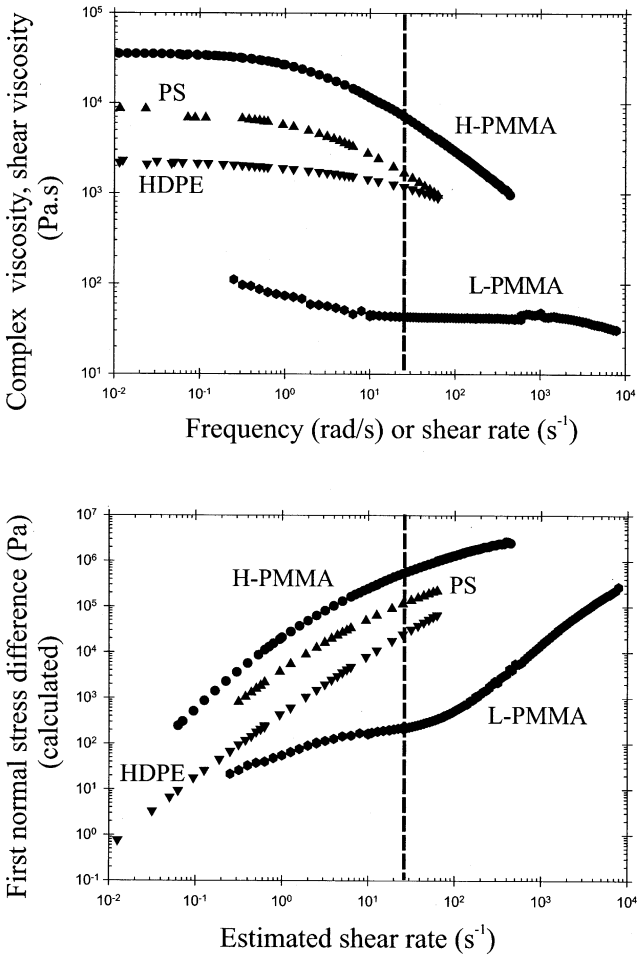

Figure 2. Complex viscosity, shear viscosity, and calculated first normal stress difference as a function of frequency or shear rate at 200°C for various homopolymers.

The dashed line represents the average shear rate in the mixer.

mode was used to measure the complex viscosity (η^*), and the storage and loss moduli (G', G'') as a function of frequency. Isothermal frequency sweep tests for the L-PMMA were carried out at various temperatures (170, 180, 190 and 200°C). By using time–temperature superposition, a master curve could be drawn at 200°C, which is the reference temperature.

The shear viscosity was estimated via an empirical relation (Cox and Merz, 1958) and verified at low shear rates. The empirical relation of Laun (1986) was used to calculate the first normal stress difference in steady shear flow. Laun demonstrated that this relation works well for many materials (linear and branched polyethylene, polypropylene, polystyrene, polyamide 6, and a PIB solution).

Since some debate still exists concerning the use of a constant shear rate or a constant shear stress in the comparison of the rheological characteristics of multiphase systems, both approaches are used in this study.

The complex viscosity as well as the viscosity and calculated first normal stress difference in steady shear flow for each of the pure melt components are plotted as a function of the frequency or shear rate in Figure 2. In the region of shear rate corresponding to the average shear rate estimated during blending ($\dot{\gamma} \cong 25\ s^{-1}$), PS and HDPE have almost the same viscosity. However, the H-PMMA is much more viscous than the other components for the whole range of shear rates, whereas the L-PMMA is much less viscous. The ranking of first normal stress difference is $N_{1,\text{H-PMMA}} > N_{1,\text{PS}} > N_{1,\text{HDPE}} > N_{1,\text{L-PMMA}}$.

Figure 3 shows the complex viscosity as well as the viscosity and calculated first normal stress difference in steady shear flow for the raw materials used as a function of the estimated shear stress. Since the pure materials follow the Cox–Merz relation, the shear stress is estimated as the product of the angular frequency and the measured complex viscosity. In the region of shear stress generated during mixing with the HDPE matrix ($\tau = 2.7 \times 10^4$ Pa), it is observed that the value of $N_{1,\text{H-PMMA}}$ becomes similar to that of the HDPE matrix. However, no significant difference appears when the viscosity of the homopolymers is compared to Figure 2.

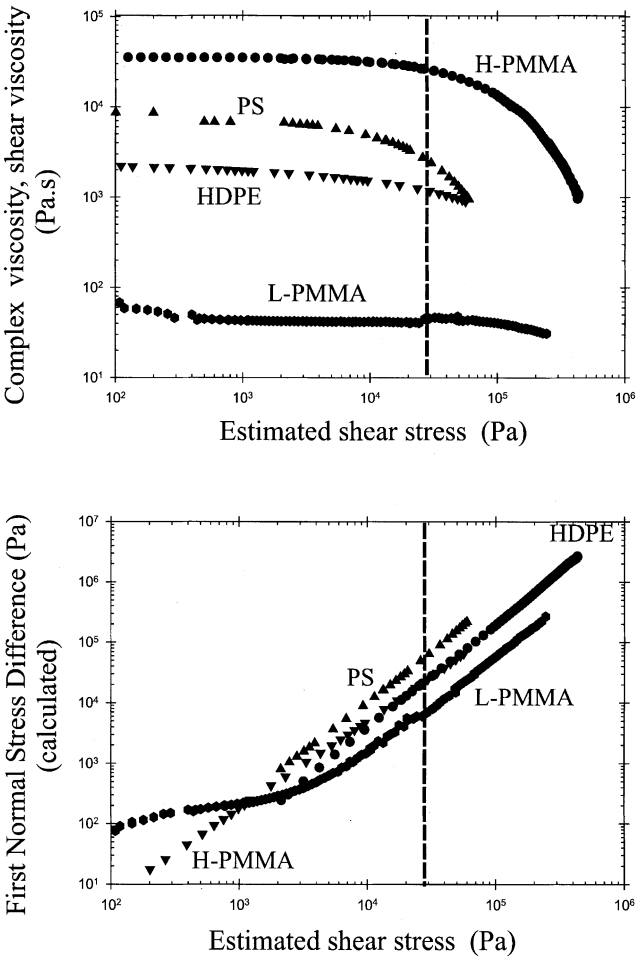

Figure 3. Complex viscosity, shear viscosity, and calculated first normal stress difference as a function of estimated shear stress at 200°C for various homopolymers.

The dashed line represents the average shear stress in the mixer.

Characterization of phase morphology

Scanning Electron Microscopy. The specimens used to investigate the composite droplet size in the ternary blend were microtomed under liquid nitrogen to create a plane face using a Leica–Jung RM 2065 microtome equipped with a glass knife. Other samples were fractured under liquid nitrogen to observe the composite droplet structure. In both cases, the samples were also subjected to the appropriate chemical treatment to selectively dissolve one of the minor phases. Cyclohexane and acetic acid were used to extract PS and PMMA, respectively, both at room temperature. After coating the desired surface with a gold–palladium alloy, the observation was carried out with a Jeol JSM 840 scanning electron microscope operated at a voltage of 10 kV.

Image Analysis. A semiautomatic method of image analysis consisting of a Wacom digitalization table and a SigmaScan Pro (Version 5.0) software was used to quantify the size and the surface fraction of the minor phase. Six fields of view and more than 1,000 diameters are analyzed later for any given point in Figures 7 and 9. Since the microtome does not necessarily cut the dispersed sphere at the widest point, a correction was applied in order to obtain the true diameter and to account for polydispersity effects (Saltikov, 1967). The volume average diameter (d_v) was obtained in this way. The typical error for the measurement of d_v is about $\pm 10\%$.

Table 2. Interfacial Tension for Immiscible Binary Systems Obtained by the Breaking-Thread Method at 200°C

Interface (Thread/Matrix)	σ (mN/m)
PS/HDPE	5.1
H-PMMA/PS	2.4
H-PMMA/HDPE	8.6

Source: Reignier and Favis (2000).

Interfacial tension measurements

The static interfacial tension data listed in Table 2 for the various polymer pairs in the ternary system were reported in a previous article (Reignier and Favis, 2000) and were measured by the breaking-thread method at 200°C with the high-

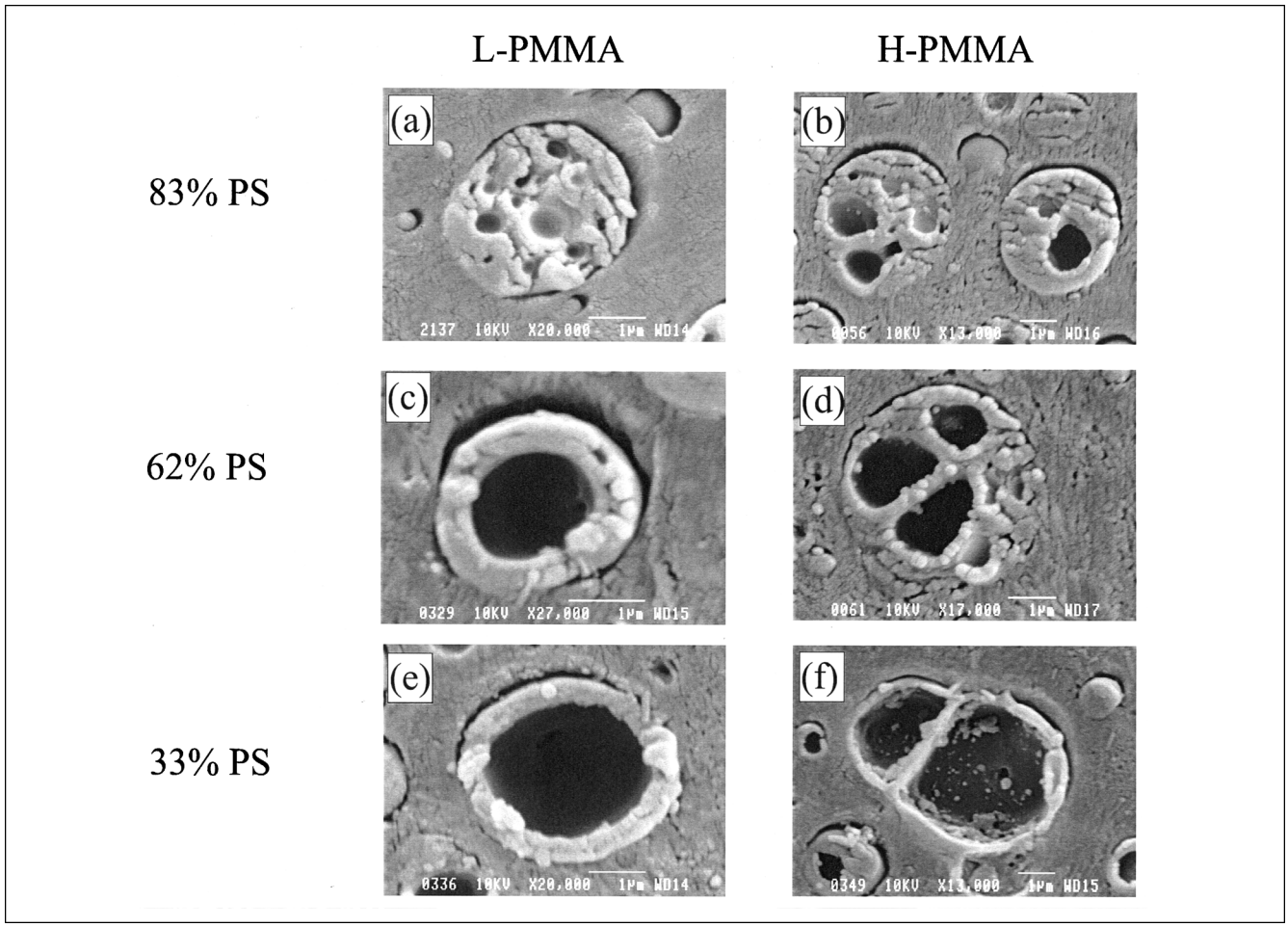

Figure 4. Evolution of the dispersed-phase internal structure as a function of the PS content (vol. % based on the dispersed phase) for the 80(HDPE)/20(PS + L-PMMA) and the 80(HDPE)/20(PS + H-PMMA) blends.

The PMMA was etched out with acetic acid. Larger than average particles visually demonstrate the internal structure of the composite droplet. The white bar equals 1 μm.

Table 3. Spreading Coefficients

Polymer Pairs	λ (mN/m)
PS/H-PMMA	2.9
H-PMMA/PS	−4.5
HDPE/PS	−12.7

Source: Reignier and Favis (2000).

molecular-weight PMMA. As discussed in a previous article (Reignier and Favis, 2003a), the interfacial tension values are not expected to change significantly when L-PMMA is used instead of H-PMMA.

These interfacial tension data were used to calculate the spreading coefficients listed in Table 3. For ternary blends of HDPE/PS/PMMA with HDPE as the matrix phase, it is predicted that PMMA particles should be completely engulfed by the PS dispersed phase.

Solvent extraction

Selective solvent extractions of PS and PMMA in cyclohexane and acetic acid, respectively, were performed for one month at room temperature for PS/PMMA blends over the whole composition range in order to determine the point of phase inversion for the PS/PMMA systems. Weight-loss measurements were carried out to calculate the extent of continuity of PS (the same equation was used for PMMA) using the following equation

$$\% \text{ Continuity} = \frac{(\text{Weight PS}_{\text{init}} - \text{Weight PS}_{\text{final}})}{\text{Weight PS}_{\text{init}}} \times 100 \quad (1)$$

The maximum error is estimated at $\pm 3\%$ continuity units.

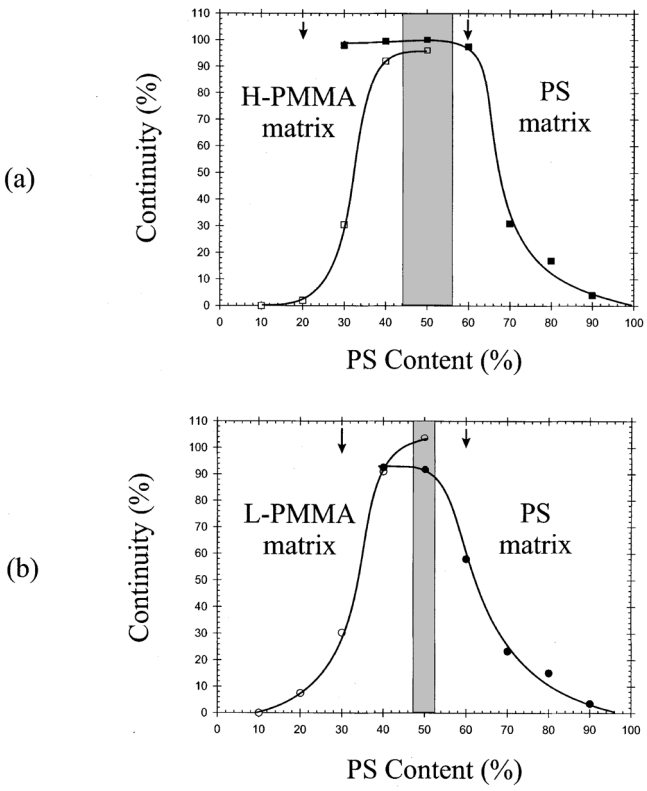

Figure 5. Degree of phase continuity vs. composition for (a) PS/H-PMMA and (b) PS/L-PMMA blends.

The gray area corresponds to the cocontinuity region. The black arrows indicate the point of disintegration of the samples.

Results and Discussion

Core–shell segregation effects

Although it was demonstrated in a previous work (Reignier and Favis, 2003a) that changing the PMMA molecular weight has no influence on the extent of composite droplet formation, it will be shown in this section that the composite droplet core molecular weight has a decisive effect on core–shell segregation effects within the composite droplet itself.

The photomicrographs reported in Figure 4 illustrate the influence of the core molecular weight on the evolution of the internal microstructure of the dispersed phase with decreasing PS/PMMA ratio for both 80 HDPE/20(PS/PMMA) systems. In comparing Figures 4a and 4c with Figures 4b and 4d, it is clearly seen that the L-PMMA system forms a core–shell morphology at significantly lower PMMA compositions than the H-PMMA case. According to Luzinov et al. (1999), the transition to a core–shell structure is the result of an impeded phase-inversion phenomenon within the composite droplet itself. In order to verify this point, the percent continuity as a function of composition was studied for binary blends of PS/L-PMMA and PS/H-PMMA in order to pinpoint their regions of dual-phase continuity. The continuity was determined via the selective solvent extraction of the PS and PMMA phases. The results are shown in Figures 5a and 5b, and it can be seen that the region of cocontinuity for both systems is centered around 50 vol. % PS. For the blend with L-PMMA, the region of cocontinuity is narrower, but no significant shift in its position is observed. It is clear that the shift in core–shell formation observed in Figure 4 is not a result of a shifting region of phase inversion resulting from the different viscosities of the PMMA.

Another important feature of Figure 4 is the presence of small droplets attached to the inner side of the PS shell in the H-PMMA blends. This point is explored further in Figure 6a, where the extraction of a portion of PMMA demonstrates the presence of a high content of entrapped particles in the high-MW-PMMA core. In Figure 6b, the microtomed surface etched for 24 h with cyclohexane clearly indicates that these subinclusions are in fact PS-phase material. Conversely, no occluded PS particles are observed in the low-MW-PMMA core, as shown in Figure 6c. Lee et al. (1997) also demonstrated the presence of a high level of shell subinclusion material in a highly viscous core of the composite droplet. Luzinov et al. (1999) interpret the presence of SBR subinclusions in a PE core as a phenomenon reminiscent of the tendency of PE to envelop SBR at PE contents larger than the theoretical phase inversion (within a PS matrix). That is not a possible explanation in the present study, since PS demonstrates a clear tendency to encapsulate PMMA. It is likely that these shell subinclusions are formed in the core during the initial stages of blending and are subsequently immobilized by the

highly viscous H-PMMA core. The immobilization of PS subinclusions in the PMMA core is also encouraged by the relatively low PS/PMMA interfacial tension.

Process of shell formation

Low-Molecular-Weight PMMA. In this part of the work, the shell formation process will be examined in detail. Initially, we will focus on the blend with the low-molecular-weight core (L-PMMA) since this system demonstrates excellent core–shell segregation effects (that is, there are very few entrapped PS particles in the PMMA core).

In order to study the shell formation process, an expression for the shell thickness is developed below. Using simple geometric arguments, it is possible to estimate the PS shell thickness for the case of dispersed spherical core–shell particles by measuring the composite droplet size and knowing the relative proportion of the core and shell phases. It is assumed that all the PMMA phase is in the composite droplet and that the composite droplet has a perfectly segregated core–shell structure. Thus, if d_v is the volume average diameter of composite droplet particles and $\phi_{PS/DP}$ the volume fraction of PS (based on the dispersed phase), the PS shell thickness H is given by

$$H = \frac{1}{2} d_v \left[1 - \sqrt[3]{(1 - \phi_{PS/DP})} \right]. \tag{2}$$

The composite droplet size as a function of the PS shell thickness is shown in Figure 7. Two main factors influence the value of the composite droplet particle size obtained at different levels of PS. First, the PS phase plays an emulsifying effect as it situates itself between the PE and the PMMA. This tends to reduce the HDPE/PMMA interfacial tension and the particle-size drops in a very similar way as a compatibilizer influences the dispersed-phase size in a classic polymer blend. Second, replacing a low-viscosity PMMA by a higher-viscosity PS at the interface tends to increase the viscosity ratio between the HDPE matrix and the composite droplet. This latter effect will tend to increase the composite droplet particle size with increasing PS composition. The opposing nature of these effects on composite droplet particle size allows for the separation of interfacial tension and viscosity ratio effects, as shown in Figure 7. That figure suggests that the full effect of interfacial tension reduction is accomplished at the minimum composite droplet particle size (14% PS), which would indicate that a complete PS layer is formed at that point. It is interesting to note that the composite droplet particle-size ratio d_v(0%PS)/d_v(14%PS) of 1.9 is virtually the same as the interfacial tension ratio of

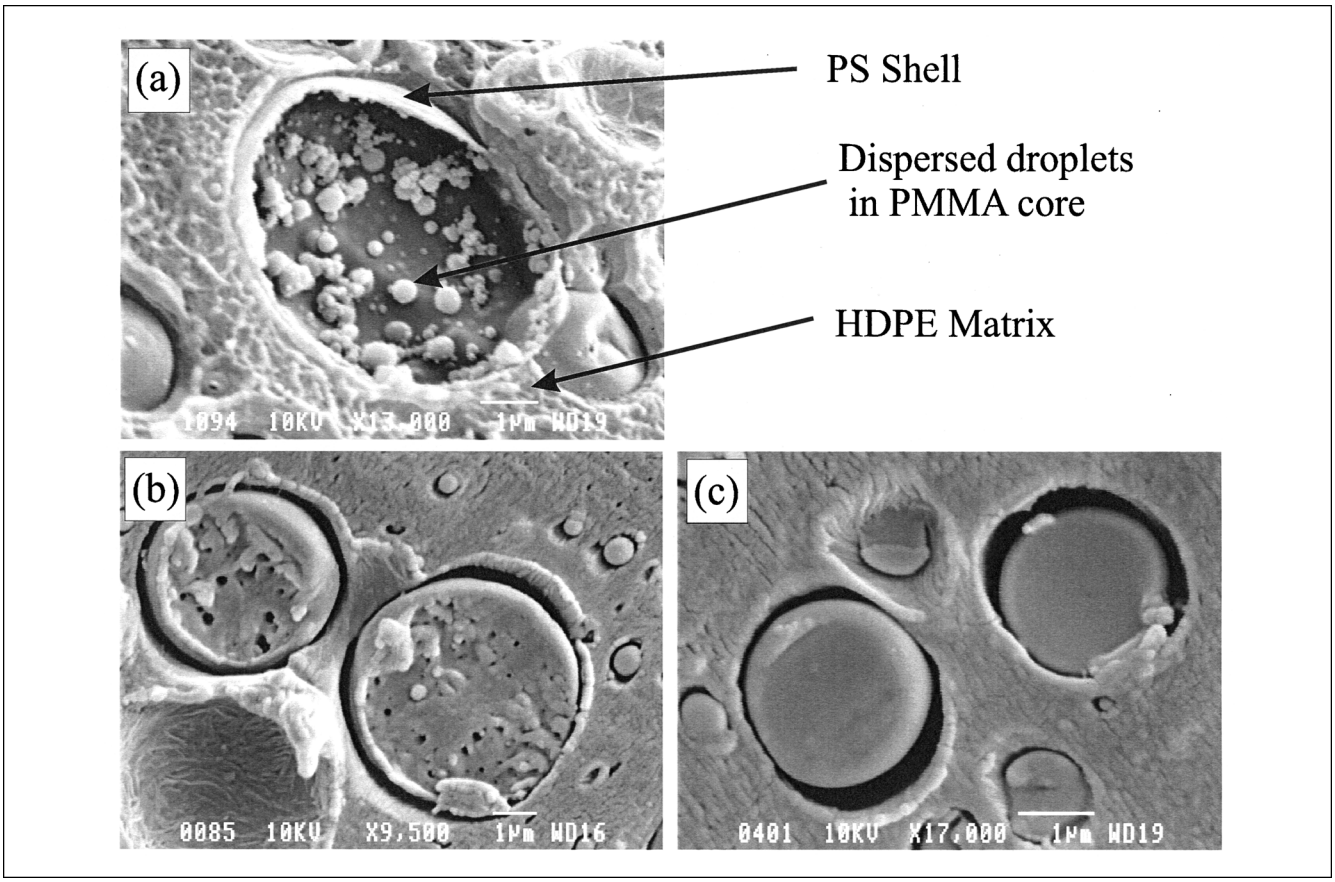

Figure 6. SEM micrographs of the 80 (HDPE)/20 (PS + PMMA).

(a) Fracture surface etched with acetic acid for 2 min, 14%PS/86%H-PMMA; (b) microtomed surface etched 24 h with cyclohexane, 9%PS/91%H-PMMA; and (c) microtomed surface etched 24 h with cyclohexane, 9%PS/91%L-PMMA.

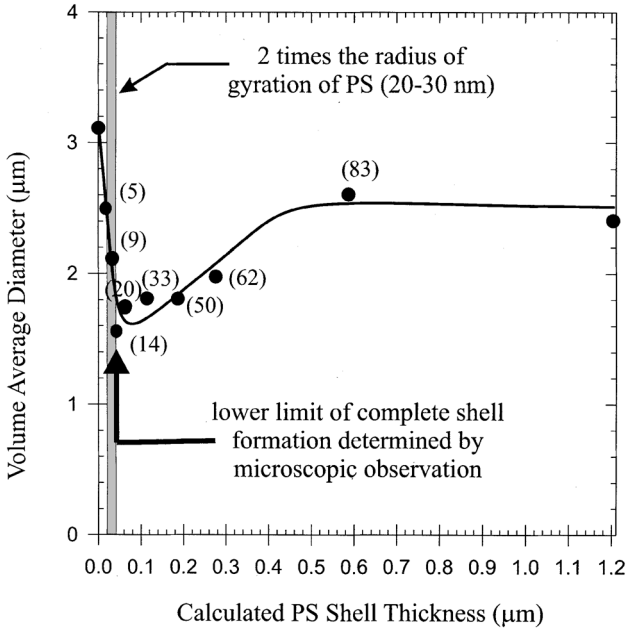

Figure 7. Dispersed-phase size as a function of the calculated PS shell thickness for the 80(HDPE)/20(PS + L-PMMA) ternary blend.

Numbers in parentheses represent the PS content based on the dispersed phase. The shell thickness is estimated from Eq. 2.

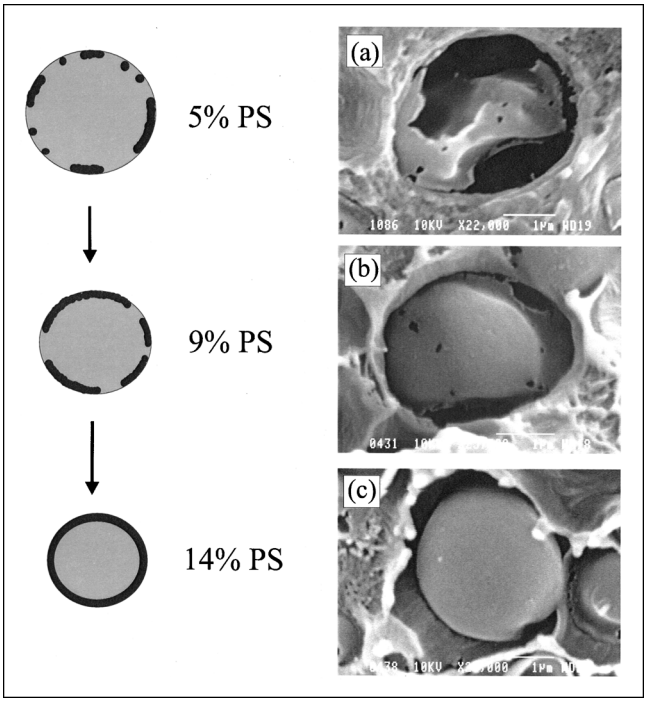

Figure 8. Evolution of the shell formation process with increasing PS content (vol. % based on the dispersed phase) for the 80(HDPE)/20(PS + L-PMMA).

In all cases, the samples were fractured under liquid nitrogen. All samples were etched for 10 s with acetic acid. Black and gray phases represent the PS and the PMMA components, respectively.

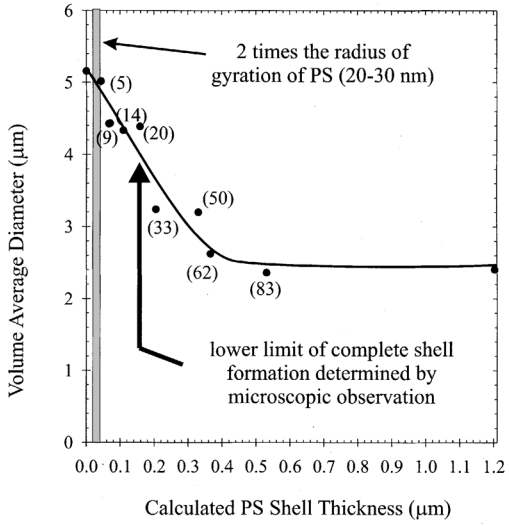

Figure 9. Dispersed-phase size as a function of the PS shell thickness for the 80(HDPE)/20(PS + H-PMMA) ternary blend.

Numbers in parentheses represent the PS content based on the dispersed phase. The shell thickness is estimated from Eq. 2.

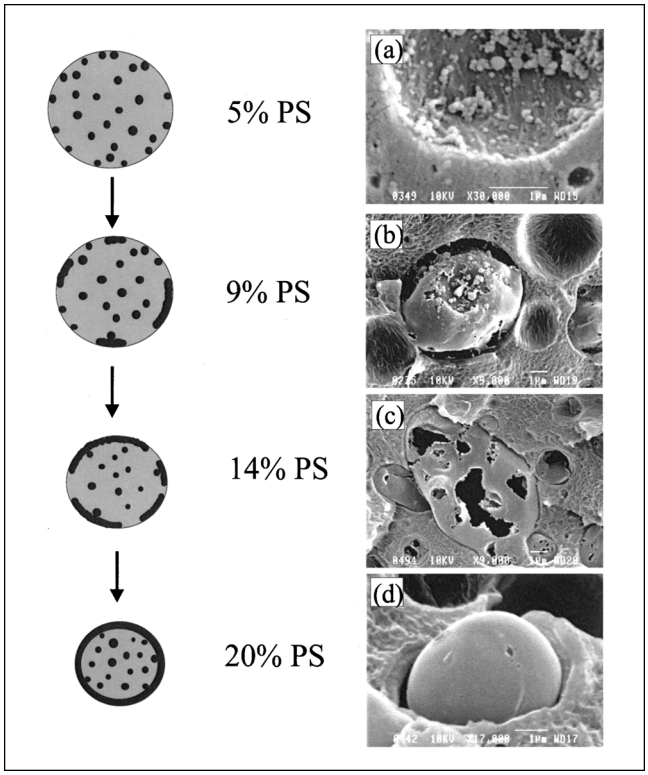

Figure 10. Evolution of the shell formation process with increasing PS content (vol. % based on the dispersed phase) for the 80(HDPE)/20(PS + H-PMMA).

In all cases the samples were fractured under liquid nitrogen. Samples (a), (c), and (d) were etched 24 h with acetic acid; (b) only 1 min to show the internal structure. Black and gray phases represent the PS and the PMMA components, respectively.

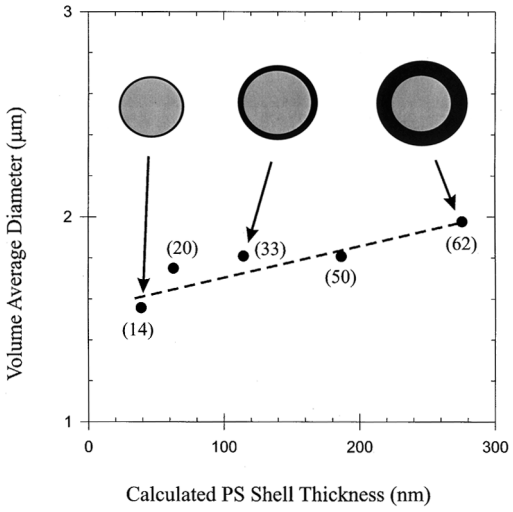

Figure 11. Control of the thickness of the PS shell at the nanometer level for the 80(HDPE)/20(PS + L-PMMA).

Black and gray phases represent the PS and the PMMA components, respectively. Numbers in parentheses represent the PS content (vol. % based on the dispersed phase).

$\sigma_{\text{H-PMMA/PE}}/\sigma_{\text{PS/PE}}$ of 1.7. Hence, the drop in particle size is closely matched by the drop in interfacial tension realized through the formation of a PS shell about PMMA. It has been shown in previous work (Lepers et al., 1997; Liang and Favis, 1999) that there is a direct relationship between dispersed particle size and interfacial tension in the absence of coalescence. This adds further support to the hypothesis that the minimum observed at 14%PS/86%L-PMMA in Figure 7 corresponds to the formation of a complete PS shell.

Microscopic observations were investigated in order to visually verify this assumption. Figure 8 shows the morphological changes of 80(HDPE)/20(PS + L-PMMA) blends for different PS compositions. The high magnification view of the particle in Figure 8a reveals that the PS shell is not complete for the blend containing 5% PS. As the PS content is increased from 9% to 14% (Figures 8b and 8c, respectively), the onset of complete shell formation is reached at 14%. Equation 2 estimates a 40-nm PS shell thickness at that concentration. This PS concentration correlates well with the minimum in particle size observed in Figure 7.

A comparison of actual shell thickness and calculated shell thickness from Eq. 2 can be carried out based on Figures 4c and 4e. As mentioned in the figure caption for Figure 4, larger than average particles are shown in order to visually demonstrate the internal structure of the composite droplet. If a particle size of 2.9 μm is used for the composite droplet in Figure 4c, the calculated shell thickness H, based on Eq. 2, would be about 0.4 μm. The measured shell thickness from Figure 4c is about 0.35 μm. The same analysis can be carried out for the particle in Figure 4e. In that case the calculated shell thickness value is about 0.3 μm, whereas the actual measured thickness is about 0.4 μm. Thus, there is a reasonable agreement between measured and actual shell thicknesses.

Furthermore, it is possible to determine the radius of gyration of the PS macromolecule by knowing the molecular weight (M_n or M_w) of the PS phase (Kuruta and Tsunashima, 1989). The results of this calculation give $R_g = 10-15$ nm based on M_n or M_w, respectively. It is remarkable that the estimated shell thickness of 40 nm for the minimum particle size composite droplet from Figure 7 compares well with two times the radius of gyration of the PS phase (20–30 nm, represented by the gray zone). This indicates that a shell of molecular thickness can be achieved for these core–shell structures.

High-Molecular-Weight PMMA. For the case of the blend possessing a high-viscosity/molecular-weight PMMA core, the effect of poor PS/PMMA segregation has a dramatic effect on the efficacy of shell formation. The composite droplet particle size as a function of added PS is shown in Figure 9. In this case both the drop in interfacial tension and the effect of viscosity ratio act to reduce the particle size as the quantity of PS is increased. It is impossible therefore to separate out the effects of these two parameters. It can be clearly seen that the composite droplet particle size diminishes up to a concentration of about 62% PS. That value represents the point where the shell thickness is sufficiently large so that the rheological behavior of the composite droplet is essentially equivalent to that of a pure PS particle. The concept of a critical shell thickness resulting in a composite droplet rheology equal to that of a dispersed phase composed of pure shell material is studied separately in another article (Reignier and Favis, 2003b).

Figure 10 shows the evolution of the PS shell formation for the 80(HDPE)/20(PS + H-PMMA) ternary blend with increasing PS content. At very low PS content (5%), where 100% represents the total volume of the composite droplet, only a few PS droplets are localized at the HDPE/PMMA interface (Figure 10a). Etching of the PMMA phase from the fracture surface shown in Figure 10b illustrates the coalescence of PS droplets into a layer that partly covers the PMMA phase. Increasing the PS content leads to a more complete PS layer. At 14% PS, only a few holes appear in the PS layer after PMMA extraction (Figure 10c). If enough PS is present at the interface (20%), a complete PS layer engulfs the PMMA phase to form a core–shell structure (Figure 10d). That value represents about 30% more PS than was observed for the system with the low viscous PMMA.

Quantitative measurement of PS shell subinclusions present in the PMMA core was investigated by measuring the surface fraction of PS shell subinclusions after extraction of the PS phase with cyclohexane. For the 80 HDPE/20(PS + H-PMMA) with a PS content of 14% (based on the composite droplet dispersed phase content), it was found that 4.8% of PS is present as subinclusions in the PMMA core, which represents about 34% of the overall PS present in the dispersed phase. This high content of PS shell subinclusions in the H-PMMA core leads to a significant decrease of the quantity of PS effectively present at the HDPE/PMMA interface and explains the delay in the formation of a complete PS shell. However, once the complete shell is formed, it is still likely of molecular scale thickness, as observed for L-PMMA.

Control of the shell thickness from nano- to microscale levels

Based on the preceding work, it is possible to derive strategies to tailor the morphology of core–shell particles with a

control of the shell thickness ranging from nano- to microscale levels. Figure 7 shows that increasing the quantity of shell material for the L-PMMA blend system, beyond the point at which a complete shell has formed, leads to an increase of the shell thickness (from 40 nm to about 1 micron), but does not contribute to further size reduction. Rather, a slight increase of the dispersed-phase size occurs because the shell viscosity is greater than the core viscosity and this changes the rheological properties of the composite droplet. In the case of the HDPE/PS/L-PMMA ternary blends, the matrix/dispersed phase viscosity ratio progressively varied from 0.02 (PMMA/HDPE system) to 1.1 (PS/HDPE system) depending on the composition of the dispersed phase. The opposing effects of reduced interfacial tension and increasing viscosity ratio result in only a small increase in composite droplet particle size with composition once the complete PS shell has formed. For this reason, it is possible to control the shell thickness of the core–shell particles through the minor phase composition ratio without substantially affecting the composite droplet particle size. Figure 11 illustrates in that case how perfectly segregated shell layers can be generated with thickness varying from 40 nm to about 300 nm.

Conclusion

This study examines the issue of core–shell morphology formation within the dispersed phase for composite droplet polymer-blend systems composed of a high-density polyethylene matrix, polystyrene shell, and different molecular weights of poly(methyl methacrylate) core material. It is shown that changing the molecular weight of the core has a dramatic effect on the PS-PMMA structure within the composite droplet. A study of the shell formation process demonstrates that the L-PMMA/PS system forms a complete PS shell structure at a significantly lower PS composition than the H-PMMA case. It was found that arguments based on the shifting of the region of phase inversion resulting from the different viscosities of the PMMA do not explain the differences in core–shell formation observed experimentally for the L-PMMA/PS and H-PMMA/PS systems.

The shift in shell formation to higher PS concentrations for the PS/H-PMMA system was attributed to a high presence of PS shell subinclusions in the PMMA core. This phenomenon was related to the high viscosity of the H-PMMA. In contrast the PS/L-PMMA system results in a perfectly segregated PS/PMMA shell–core structure. No occluded PS particles are observed in the PMMA core. In that last case, a direct microscopic study of the process of shell formation clearly demonstrates that the onset of complete PS shell formation corresponds to the minimum observed in particle size and that, at this point, the PS shell thickness is equal to about two times the radius of gyration of PS. Thus, the thinnest possible shell in such a system possesses a molecular-scale thickness. Perfectly segregated shell layers ranging from 40 nm to 300 nm thickness can be obtained for the PS/L-PMMA blend system through the control of the PS/PMMA composition ratio with virtually no change in the overall composite droplet diameters.

Acknowledgments

The authors thank Pei Lian Ma for fruitful discussions.

Literature Cited

Berger, W., H. W. Kammer, and C. Kummerlöwe, "Melt Rheology and Morphology of Polymer Blends," *Makromol. Chem.*, Suppl. 8, 101 (1984).

Cox, W. P., and E. H. Merz, "Correlation of Dynamic and Steady Flow Viscosities," *J. Poly. Sci.*, **28**, 619 (1958).

Favis, B. D., and J. P. Chalifoux, "Influence of Composition on the Morphology of Polypropylene/Polycarbonate Blends," *Polymer*, **29**, 1761 (1988).

Favis, B. D., C. Lavallee, and A. Derdouri, "Preparation of Composite Dispersed Phase Morphologies in Incompatible and Compatible Blends During Melt Mixing," *J. Mater. Sci.*, **27**, 4211 (1992).

Gupta, A. K., and K. R. Srinivasan, "Melt Rheology and Morphology of PP/SEBS/PC Ternary Blend," *J. Appl. Polym. Sci.*, **47**, 167 (1993).

Hobbs, S. Y., M. E. J. Dekkers, and W. H. Watkins, "Effect of Interfacial Forces on Polymer Blend Morphologies," *J. Mater. Sci.*, **23**, 1598 (1988).

Kurata, M., and Y. Tsunashima, *Polymer Handbook*, 3rd ed., Chap. VII, J. Brandrup and E. H. Immergut, eds., Wiley, New York (1989).

Laun, H. M., "Prediction of Elastic Strains of Polymer Melts in Shear and Elongation," *J. Rheol.*, **30**(3), 459 (1986).

Lee, M. S., T. P. Lodge, and C. W. Macosko, "Can Random Copolymers Serve as Effective Polymeric Compatibilizers?," *J. Poly. Sci.: Part B: Poly. Phys.*, **35**, 2835 (1997).

Lepers, J. C., B. D. Favis, and R. J. Tabar, "The Relative Role of Coalescence and Interfacial Tension in Controlling Dispersed Phase Size Reduction During the Compatibilisation of Polyethylene Terephthalate/Polypropylene Blends," *J. Poly. Sci.: Part B: Poly. Phys.*, **35**, 2271 (1997).

Liang, H., B. D. Favis, Y. S. Yu, and A. Eisenberg, "Correlation Between the Interfacial Tension and Dispersed Phase Morphology in Interfacially Modified Blends of LLDPE and PVC," *Macromolecules*, **32**, 1637 (1999).

Luzinov, I., K. Xi, C. Pagnoulle, G. Huynh-Ba, and R. Jérôme, "Composition Effect on the Core-Shell Morphology and Mechanical Properties of Ternary Polystyrene/Styrene-Butadiene Rubber/Polyethylene Blends," *Polymer*, **40**, 2511 (1999).

Marquez, L., J. Quijano, and M. Gaulin, "A Calibration Technique to Evaluate the Power-Law Parameters of Polymer Melts Using a Torque-Rheometer," *Poly. Eng. Sci.*, **36**, 2556 (1996).

Reignier, J., and B. D. Favis, "Control of the Subinclusion Microstructure in HDPE/PS/PMMA Ternary Blends," *Macromolecules*, **33**, 6998 (2000).

Reignier, J., B. D. Favis, and M. C. Heuzey, "Factors Influencing Encapsulation Behavior in Composite Droplet-Type Polymer Blends," *Polymer,* **44**, 49 (2003a).

Reignier, J., and B. D. Favis, "On the Presence of a Critical Shell Volume Fraction Leading to Pseudo-Pure Droplet Behavior in Composite Droplet Polymer Blends," *Polymer* (2003b).

Saltikov, S. A., "The Determination of the Size Distribution of Particles in an Opaque Material from a Measurement of the Size Distribution of their Section," *Proc. Int. Cong. for Stereology*, Helias, New York (1967).

Torza, S., and S. G. Mason, "Three-Phase Interactions in Shear and Electrical Fields," *Colloid Sci.*, **33**, 67 (1970).

Van Oene, H., "Mode of Dispersions of Viscoelastics Fluids in Flow," *J. Colloid Interface Sci.*, **40**, 448 (1972).

Manuscript received May 20, 2002, and revision received Sept. 18, 2002.